Analytical Biochemistry 390 (2009) 141–148

Contents lists available at ScienceDirect

Analytical Biochemistry

journal homepage: www.elsevier.com/locate/yabio

Tracking and quantification of ^{32}P-labeled phosphopeptides in liquid chromatography matrix-assisted laser desorption/ionization mass spectrometry

Roland D. Tuerk [a], Yolanda Auchli [b], Ramon F. Thali [a], Roland Scholz [a], Theo Wallimann [a], René A. Brunisholz [b,*,1], Dietbert Neumann [a,*,1]

[a] Institute of Cell Biology, Department of Biology, ETH Zurich, 8093 Zurich, Switzerland
[b] Functional Genomics Center Zurich (FGCZ), University of Zurich, 8057 Zurich, Switzerland

ARTICLE INFO

Article history:
Received 2 February 2009
Available online 17 April 2009

Keywords:
AMP-activated protein kinase
Autophosphorylation
LC–MALDI MS
Radiolabeling
Prespotted AnchorChip

ABSTRACT

Phosphoamino acid modifications on substrate proteins are critical components of protein kinase signaling pathways. Thus, diverse methodologies have been developed and applied to identify the sites of phosphorylated amino acids within proteins. Despite significant progress in the field, even the determination of phosphorylated residues in a given highly purified protein is not a matter of routine and can be difficult and time-consuming. Here we present a practicable approach that integrates into a liquid chromatography matrix-assisted laser desorption/ionization mass spectrometry (LC–MALDI MS) workflow and allows localization and quantification of phosphorylated peptides on the MALDI target plate prior to MS analysis. Tryptic digests of radiolabeled proteins are fractionated by reversed-phase LC directly onto disposable MALDI target plates, followed by autoradiographic imaging. Visualization of the radiolabel enables focused analysis of selected spots, thereby accelerating the process of phosphorylation site mapping by decreasing the number of spectra to be acquired. Moreover, absolute quantification of the phosphorylated peptides is permitted by the use of appropriate standards. Finally, the manual sample handling is minimal, and consequently the risk of adsorptive sample loss is very low. Application of the procedure allowed the targeted identification of six novel autophosphorylation sites of AMP-activated protein kinase (AMPK) and displayed additional unknown phosphorylated peptide species not amenable to detection by MS. Furthermore, autoradiography revealed topologically inhomogeneous distribution of phosphorylated peptides within individual spots. However, accurate analysis of defined areas within single spots suggests that, rather than such quantitative differences, mainly the manner of matrix crystallization significantly affects ionization of phosphopeptides.

The actions of protein kinases and phosphatases, which result in the reversible phosphorylation of proteins at the serine (Ser),[2] threonine (Thr), and tyrosine (Tyr) residues, are key signaling events in eukaryotic cells and regulate a plethora of important biological processes such as cell division, metabolic maintenance, inter- and intracellular signal transduction, and programmed cell death [1–3]. It is supposed that 30% of all proteins in eukaryotic cells exist in a phosphorylated state at any given time [4,5], reflecting the abundance and significance of this protein modification. To elucidate the functional consequences of such phosphorylation events, a common strategy involves mutagenesis of the targeted residues to mimic either the presence or absence of phosphorylation. In addition, antibodies that specifically recognize the phosphorylated residues are powerful tools to track the phosphorylation state of the investigated target protein in situ and to characterize kinase–substrate interactions down to the mechanistic level [6,7]. A mandatory prerequisite of such techniques, however, is to obtain knowledge of the phosphorylation sites.

Due to their sensitivity and reliability, as well as their suitability for high-throughput applications, mass spectrometry (MS)-based methods of determining phosphorylation sites on proteins have become increasingly popular [8]. Major difficulties in MS-based analysis of phosphorylation emanate from two phenomena. First, detection of phosphopeptides is often hindered by suppression ef-

* Corresponding authors. Fax: +41 0 44 633 10 69 (D. Neumann), +41 0 44 635 39 22 (R.A. Brunisholz).
E-mail addresses: rene.brunisholz@fgcz.ethz.ch (R.A. Brunisholz), dietbert.neumann@cell.biol.ethz.ch (D. Neumann).

[1] These authors contributed equally to this work.

[2] *Abbreviations used:* Ser, serine; Thr, threonine; Tyr, tyrosine; MS, mass spectrometry; LC, liquid chromatography; IMAC, immobilized metal ion affinity chromatography; RPLC, reversed-phase LC; ESI, electrospray ionization; MALDI, matrix-assisted laser desorption/ionization; AMPK, AMP-activated protein kinase; CHCA, α-cyano-4-hydroxy-cinnamic acid; TOF, time-of-flight; DA–AMPK, kinase-deficient AMPK; MO25α, mouse protein 25 α; STRADα, STE-20-related adaptor protein α; PAC, Prespotted AnchorChip; SDS, sodium dodecyl sulfate; PAGE, polyacrylamide gel electrophoresis; TFA, trifluoroacetic acid; 1D, one-dimensional; MS^2, tandem mass spectrometry; PMF, peptide mass fingerprint; CamKKβ, calmodulin-dependent protein kinase kinase β; LE, exemption limit.

0003-2697/$ - see front matter © 2009 Elsevier Inc. All rights reserved.
doi:10.1016/j.ab.2009.04.015

fects [9]. Second, the probability that phosphopeptides are masked by isobaric peptides rises with increasing sample complexity. Hence, phosphopeptides must be separated from the bulk of non-phosphorylated peptides prior to analysis by MS—a task that is most often accomplished with liquid chromatography (LC). Immobilized metal ion affinity chromatography (IMAC) is a widely used LC-based approach to enrich for phosphorylated peptides [10,11]. Although allowing purification of hundreds of phosphopeptides from highly complex mixtures such as whole cell lysates, peptide binding to these column matrices is not exclusively specific for phosphopeptides. More important, considerable sample loss (i.e., poor phosphopeptide recovery) can occur [12]. The latter is highly unfavorable, particularly in our case when the identification of not only some but all phosphorylation sites of single isolated proteins is demanded. Reversed-phase LC (RPLC) is another method for the separation of peptides and is based on their hydrophobic character. A common constraint with this type of column material is that small hydrophilic phosphopeptides are hardly retained and elute with nonbinding salts and buffers. Unlike electrospray ionization (ESI), however, matrix-assisted laser desorption/ionization (MALDI) exhibits a relatively high tolerance to salts and buffers and, therefore, is better suited for the analysis of such flow-through fractions [13]. The determination of phosphorylation sites within proteins frequently includes labeling with ^{32}P before proteolytic digestion, followed by RPLC and fraction collection into microfuge tubes. The ^{32}P label can be traced by scintillation counting, thereby pinpointing to fractions that contain the phosphopeptides of interest. Often, these fractions are too dilute and require an additional concentrating step prior to MS analysis. Although this workflow has been applied successfully in numerous studies, major disadvantages arise because of the time-consuming and laborious manual handling and because of substantial sample loss due to repeated interactions with plastic surfaces such as pipet tips and microcentrifugation tubes [14]. In addition, insufficient peptide recovery from vacuum-dried samples can account for up to 50% adsorptive loss [14,15].

To minimize critical sample loss and manual intervention, we investigated alternative techniques for phosphorylation site mapping without abandoning the advantages of peptide radiolabeling and separation. Notably, we put our emphasis on analysis of in vitro phosphorylation using purified proteins. In the current study, we describe an LC–MALDI MS workflow featuring autoradiographic imaging of MALDI target plates. Because we are aware of safety issues that have diminished the use of radioactivity in several laboratories, it is necessary to point out that this approach requires only marginal use of radioactivity due to the exquisite sensitivity of the detection method. The technique offers visualization and tracking of phosphorylated peptides and, thus, facilitated the targeted identification of several novel autophosphorylation sites of AMP-activated protein kinase (AMPK), an important and central regulator of cellular energy balance.

Materials and methods

Materials

[γ-^{32}P]ATP was purchased from Hartmann Analytic (Braunschweig, Germany). Amersham Hyperfilm MP autoradiography films were obtained from GE Healthcare (Otelfingen, Switzerland). Trypsin was purchased from Promega (Wallisellen, Switzerland). Prespotted AnchorChip target plates (PAC384, cat. no. 227463) with 384 prespotted α-cyano-4-hydroxy-cinnamic acid (CHCA) spots/96 prepared calibrant spots and the Ultraflex time-of-flight (TOF)/TOF II MALDI mass spectrometer were obtained from Bruker Daltonics (Bremen, Germany). Recombinant $\alpha1\beta1\gamma1$ or His-$\alpha1\beta1\gamma1$ isotypes of kinase-deficient AMPK (DA–AMPK) and wild-type AMPK were expressed in *Escherichia coli* and purified as published previously [16–18]. DA–AMPK is characterized by an aspartate-to-alanine mutation at position 157 of the $\alpha1$ subunit that disrupts the Mg^{2+} ATP binding of the catalytic subunit and, therefore, renders the kinase inactive [19]. Bacterial expression and purification of the heterotrimeric LKB1 complex consisting of the tumor suppressor kinase LKB1, the scaffolding protein mouse protein 25 α (MO25α), and the pseudokinase STE-20-related adaptor protein α (STRADα) was performed as described previously [17,20]. All other chemicals and reagents were obtained from standard suppliers.

Determination of the X-ray film sensitivity

The maximum theoretical specific activity of ^{32}P (i.e., if every ATP molecule were labeled) is 9131 Ci/mmol or 337.847 TBq/mmol. Therefore, an activity of 1 Bq corresponds to 2.96 amol ^{32}P (2.96×10^{-18} mol ^{32}P). For simplicity, we used a value of 3 amol/Bq in the figure denotations. A dilution series of the purchased [γ-^{32}P]ATP solution was manually applied in aliquots of 1 µl onto a Prespotted AnchorChip (PAC) and allowed to dry at room temperature. Subsequently, an autoradiography film was exposed for 24 h with the additional aid of an intensifying tungstate screen. Afterward, a new film was exposed for 2 weeks in the same manner.

Phosphorylation of DA–AMPK by LKB1

Bacterially expressed DA–AMPK (2.5 µg) was phosphorylated by LKB1–MO25α–STRADα (100 ng) at 37 °C in kinase buffer supplemented with [γ-^{32}P]ATP (specific activity of 16 Bq/pmol ATP) at a volume of 50 µl. The reaction was allowed to proceed for 2 h and was stopped by adding 10 µl of sodium dodecyl sulfate (SDS) sample buffer (105 mM Tris–HCl [pH 6.8], 4% [w/v] SDS, 15% [v/v] glycerol, 1.2 M 2-mercaptoethanol, and 0.02% [w/v] bromophenol blue) and heating to 95 °C for 5 min. Following SDS–polyacrylamide gel electrophoresis (PAGE) and Coomassie-blue staining, gels were air-dried between two layers of cellophane and exposed to autoradiography films. The dried gel band corresponding to the $\alpha1$ subunit of AMPK was excised and rehydrated in water. Subsequently, the cellophane layers were removed and the gel pieces were subjected to in-gel digestion with trypsin as described previously [21]. The extracted peptides were concentrated in a centrifugal vacuum concentrator to a volume of 10 µl and stored at −20 °C until further use.

Autophosphorylation of AMPK

To promote autophosphorylation, recombinant His-tagged $\alpha1\beta1\gamma1$–AMPK (5 µg) or nontagged $\alpha1\beta1\gamma1$ (2 µg) was incubated with LKB1–MO25α–STRADα (100 ng) at 37 °C in kinase buffer containing [γ-^{32}P]ATP (specific activity of 16 Bq/pmol ATP). The final volume of the reaction mix was 50 µl. The reaction was allowed to proceed for 2 h and was further processed as described above except that the two AMPK–$\beta1$ bands were also excised.

Capillary LC and microfractionation onto PACs

Small amounts (1–5 µl) of the concentrated tryptic peptides were applied to a microbore reversed-phase column (ZORBAX SB C_{18}, bead size 3.5 µm, pore size 300 Å, 150 × 0.5 mm [length × i.d.], Agilent Technologies, Santa Clara, CA, USA) connected to an Agilent 1100 capillary LC system that was equipped with a microcollection/spotting system. If not otherwise mentioned in the figure legends, the separation of the peptides was achieved using 0.1% (v/v) trifluoroacetic acid (TFA) in water (solvent A) and 97% (v/v) acetonitrile containing 0.1% (v/v) TFA (solvent B). A gradient was applied

by increasing solvent B from 5% to 25% over 25 min, followed by an increase of solvent B up to 95% over an additional 15 min. A slightly steeper gradient was applied to separate the peptides derived from digestion of nontagged α1–AMPK, starting from 5% B to 45% B over 35 min, followed by a linear solvent B increase up to 95% B over 10 min. The total run time, including washing and reequilibration to starting conditions, was 72 min. The flow rate was 7 μl/min, and peptide separation was monitored at 220 and 280 nm. Fraction deposition was every 20 s, yielding a fraction volume of 2.33 μl.

Autoradiography of PACs and quantification of phosphopeptides

After the run, the PAC was allowed to dry at room temperature and exposed to autoradiography films with the aid of an intensifying tungstate screen. The films were carefully applied to the PAC targets without any further adjustment once they were overlaid. Autoradiographs were digitalized as high-resolution TIFF files (1200 dpi), and spots were quantified by densitometry using Kodak digital science one-dimensional (1D) image analysis software (version 2.0.4, Kodak, Renens, Switzerland). For absolute quantification, a dilution series of the radioactive kinase buffer used in the phosphorylation reaction was manually spotted in triplicate onto the PAC prior to autoradiographic imaging. After densitometric analysis, the mean signal intensities were plotted versus the actual amounts of ^{32}P and a linear regression was performed. Both mean signal intensities and standard deviations were calculated from three measurements. The function of the regression line was used to back-calculate the absolute amounts of phosphopeptide from the signal intensities of each spot.

Mass spectrometry

After autoradiography, selected fractions of the PAC target indicating the presence of radiolabeled phosphopeptides were analyzed by MALDI MS and MALDI tandem MS (MS^2) using an upgraded Bruker Daltonics Ultraflex TOF/TOF II MALDI mass spectrometer with the control and analysis software Compass (version 1.2, also from Bruker Daltonics). The frequency-tripled Nd:YAG laser at 355 nm, using a structured focus profile (smartbeam, Bruker Daltonics), was set to a repetition rate of 50 Hz, and the ion acceleration voltage was 25 kV. The mass measurements were performed in the positive ion reflector mode with 150 ns as the delayed extraction time. All spectra were manually recorded with approximately 500 to 1000 accumulated single laser shots and were externally calibrated with the mass signals of the incorporated peptide calibrant standard of the PAC. The first monoisotopic signals in the spectra were assigned automatically using the peak detection algorithm SNAP (Bruker Daltonics), and the smoothing algorithm of Savitzky–Golay was applied (width 0.2 *m/z,* cycle number 1). For fragmentation of selected peptides by MS^2, we applied the LIFT technology from Bruker Daltonics [22]. The MS^2 spectra were transferred to the MS Biotools program (version 3.0, Bruker Daltonics) and compared with the in silico digested α1 or β1 subunit of AMPK with the aid of the sequence editor software from Bruker Daltonics. The mass tolerance of the MS^2 measurements was set at 0.5 Da in the Biotools software. The comparison parameters tolerated phosphorylation of serine and threonine, oxidation of methionine, and derivatization of cysteine to carbamidomethyl cysteine or propionamide cysteine as variable modifications. To find phosphopeptides, we first acquired a peptide mass fingerprint (PMF) and then applied one of three alternative strategies. First, the experimental masses were compared with a theoretical mass list of tryptic AMPK–α1 or AMPK–β1 peptides that was generated in silico. Any observed masses that matched to computed phosphopeptides were then selected for MS^2, in which phosphorylated peptide ions undergo a preferential neutral loss of the elements of orthophosphoric acid (H_3PO_4, 98 Da) or metaphosphoric acid (HPO_3, 80 Da). Such metastable fragmentation of peptides phosphorylated at serine or threonine can also be observed in the PMF when MALDI MS is performed in the reflector mode [23]. Hence, the second strategy to select ions for MS^2 was to look for ion pairs with characteristic mass differences of 98 or 80 Da in the PMF, suggesting the presence of a phosphorylated peptide along with its related species after neutral loss. If both strategies failed, we scanned every single ion from the PMF for a neutral loss in MS^2 mode, a task that was not overly laborious due to the limited number of radioactive spots to be analyzed.

Analysis of heterogeneous PAC spots

Four different PAC spots were selected for phosphopeptide isolation—but not fragmentation—in MS^2 mode. Within each spot, the laser was manually locked into 13 different positions for data acquisition. The laser intensity was set to 30% power, and 400 shots were accumulated for each spectrum. The different signal intensities for the isolated phosphopeptide (parent ion) at the various positions were graphed with SigmaPlot from Systat Software (San Jose, CA, USA).

Results and discussion

Implementation of in situ autoradiography into the LC–MALDI MS workflow

Peptides produced by proteolytic digestion of radiolabeled proteins are fractionated by RPLC directly onto disposable PACs containing 384 spots with CHCA and 96 calibrant spots (Fig. 1A). Although ordinary MALDI target plates can also be used for fractionation, we took advantage of the disposable PACs because they are intended for single use and, therefore, eliminate the risk of memory effects. Radiolabeled phosphopeptides are detected in situ by exposing an X-ray film to the PAC, thereby allowing unambiguous assignment of their exact localization on the target plate (Fig. 1B). Hence, only particular spots are selected for in-depth analysis by MS and MS^2. An additional important benefit of the autoradiographic detection is provided by the excellent sensitivity of X-ray films, which have a detection limit for ^{32}P in the lower zeptomole (10^{-21}) range, that is, a few thousand atoms per spot (Fig. 2). Moreover, the resolution allows visualization of the phosphopeptide distribution pattern within a spot, which can sometimes be rather heterogeneous (Fig. 1B, inset).

Analysis of AMPK autophosphorylation

We used the methodology described above to identify the autophosphorylation sites of AMPK. AMPK is a central regulator of energy homeostasis at the cellular and whole-body level and has recently emerged as an important mediator of the beneficial effects exerted by metformin, a drug that is widely used to treat type 2 diabetes [24]. AMPK is a heterotrimeric kinase comprising a catalytic α subunit and regulatory β and γ subunits. It is activated via phosphorylation at Thr172 of the α subunit by Ca^{2+}/calmodulin-dependent protein kinase kinase β (CamKKβ) or the tumor suppressor LKB1 [25]. As reflected by reduced electrophoretic mobility on activation [17], AMPK also undergoes autophosphorylation of the α and β subunits, thereby adding further important levels of regulation [26]. However, in-depth knowledge of its autoregulation, which likely includes hitherto unknown phosphorylation sites, is still lacking.

To investigate AMPK autophosphorylation, we incubated 5 μg of α1β1γ1–AMPK with 100 ng of LKB1 complex in the presence of [γ-^{32}P]ATP. Following protein separation by SDS–PAGE,

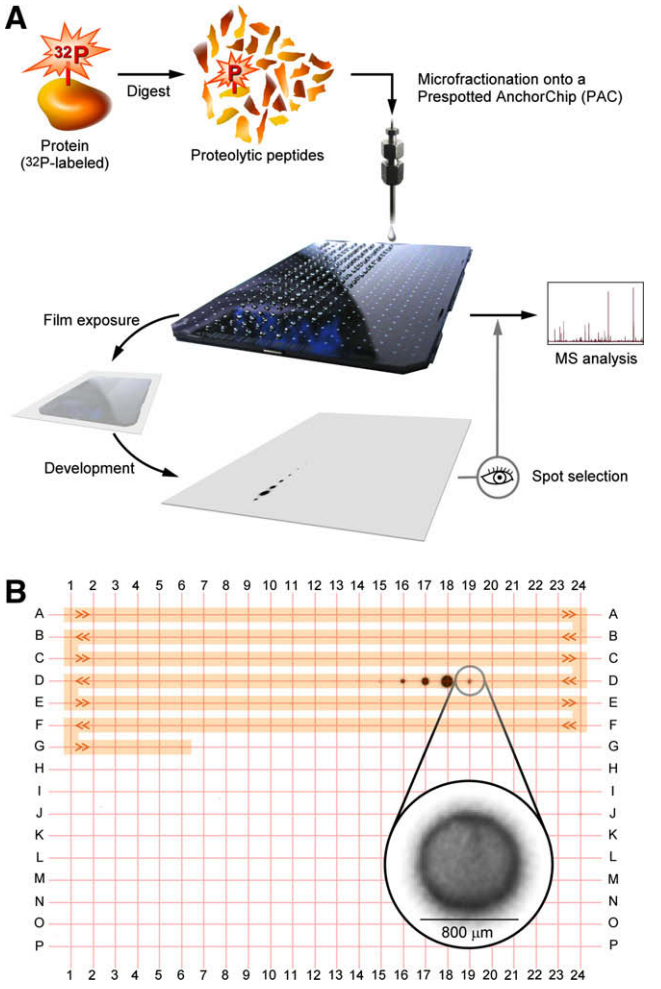

Fig. 1. Workflow illustrating the sequential use of autoradiography and LC–MALDI MS for phosphorylation site mapping. (A) Proteolytic digests of ^{32}P-labeled proteins are fractionated by RPLC and spotted directly onto PACs. After autoradiographic detection of the radiolabeled phosphopeptides in situ (i.e., on the chip surface), only relevant spots are analyzed in more detail by MS. (B) In addition to revealing the exact position of the phosphopeptides on the target plate, the irregular distribution of labeled peptides within a single spot due to nonuniform cocrystallization of sample and matrix emerges after short film exposure (see enlarged spot in the inset).

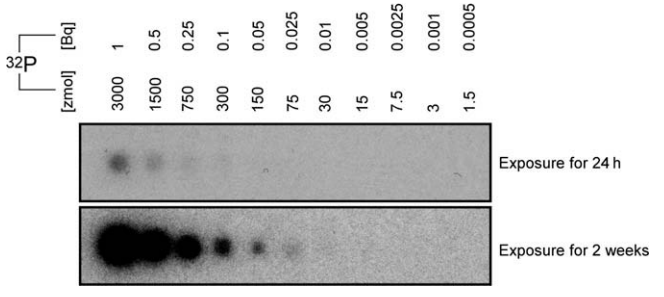

Fig. 2. Sensitivity of the X-ray films for visualization of ^{32}P. An aqueous dilution series of [γ-^{32}P]ATP was manually spotted onto a PAC and exposed to an autoradiography film for 24 h (upper panel) or for 2 weeks (lower panel). After 24 h, 1 Bq of activity was already clearly detectable. A maximal sensitivity of 0.01 Bq, corresponding to 30 zmol of ^{32}P, was observed after 2 weeks.

Coomassie staining, and gel drying, incorporation of ^{32}P was visualized by autoradiography (Fig. 3A). As expected, the α1 and β1 subunits of AMPK were strongly labeled (Fig. 3A, α1 and β1A). However, we also observed predominant ^{32}P incorporation into a β1 species of slower electrophoretic mobility (Fig 3A, β1B). After tryptic in-gel digestion of the appropriate protein bands, approximately one-quarter of the digest was separated by RPLC and spotted onto the PACs in 2.3-µl fractions. Although only two autophosphorylation sites on the α1 subunit have been described to date [27], autoradiographic detection of the radiolabeled phosphopeptides on the chip (Fig. 3B) and densitometric analysis of the same X-ray film (Fig. 3C) revealed 11 ^{32}P peaks, each corresponding to a different phosphopeptide species of the α1 subunit. Not surprisingly, the autoradiographic image of the β1B elution pattern differed from that of β1A by the appearance of additional radioactive spots (Fig. 3B). Although the two dominant β1A-derived peaks were also observed in the fractionated digest of β1B with similar retention times (Fig. 3C, cf. A6/E5 with G20/K21), five radiolabeled positions were exclusive to the peptides originating in the β1B band (Fig. 3C, fractions H8, J12, J6, K14, and K16), underlining that additional phosphorylation events on AMPK–β1 were responsible for the reduced electrophoretic mobility of β1B. In total, we were able to unambiguously map 10 different phosphorylation sites on AMPK (Table 1; see also Supplementary MS Data S1 in supplementary material). Because the activating kinase LKB1 phosphorylated AMPK exclusively at [α1]Thr172 (Supplementary Fig. S1), all of the other residues represented bona fide autophosphorylation sites. In addition to the previously reported sites [α1]Ser485, [β1]Ser24, and [β1]Ser108, we identified six novel autophosphorylation sites of AMPK (Table 1).

Six phosphorylation sites of AMPK–α1 were identified, although 11 separate, HPLC-derived ^{32}P peaks were observed (Fig. 3C and Table 1). Several different circumstances contributed to this result. First, two phosphopeptides remained unidentified (G9 and K22). Second, the two sites of the monophosphorylated peptides in fraction J17 were also found in an individual, doubly phosphorylated peptide in fraction J21. Third, the phosphorylation site corresponding to Thr377 was identified in three distinct peptide species, slightly differing due to a missed cleavage site and an unknown modification characterized by a mass deviation of 1 Da (J1, K2, and K5). Furthermore, the phosphopeptide in fraction G21 derived from the N-terminal hexahistidine tag and, therefore, was not classified as a true AMPK autophosphorylation site. In contrast to the α1 subunit, fractionation of the β1 peptides resulted in a less complex radioactive elution pattern and fewer redundant matches (Fig. 3C and Table 1). Indeed, MS analysis of these radioactive spots revealed that every ^{32}P peak represented a unique phosphorylation site. Even phosphopeptides that were not retained on the RP column but eluted in the flow-through fractions were unambiguously identified (Fig. 3C, A6 and G20).

Absolute quantification of phosphopeptides after spotting

Knowledge of the absolute peptide amounts that are analyzed by MALDI MS is crucially important in some applications. For instance, such quantitative information is fundamental for optimization of the ionization efficiency of phosphopeptides by using different crystal matrices or matrix additives [28–30]. Indeed, densitometric analysis of the autoradiographs not only provides information regarding the positions and relative amounts of phosphopeptides on the PACs but can also be used to determine their absolute quantity within individual spots. We reanalyzed autophosphorylation of AMPK–α1 and quantified the amount of phosphopeptides per spot by using appropriate ^{32}P standards on the PAC (Fig. 4). Depending on the nature of the peptides, successful phosphorylation site identification required varying amounts. For example, 23 fmol of the phosphopeptide SGpSISNYR already allowed parent ion isolation and detection of the loss of orthophosphoric acid (H_3PO_4) in MS^2 mode, and only 34 fmol of this peptide was sufficient to clearly pinpoint the phosphorylated residue

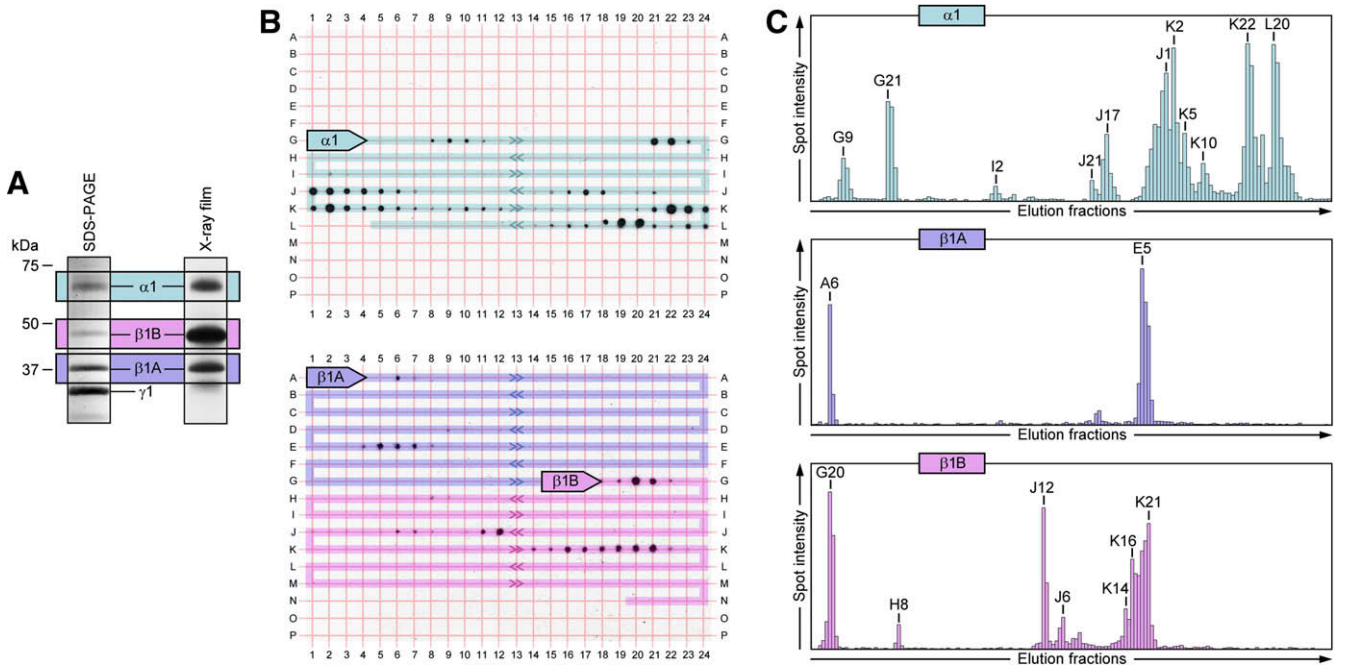

Fig. 3. Analysis of AMPK autophosphorylation sites. (A) Bacterially expressed trimeric His-α1β1γ1–AMPK (5 μg, His-tagged) was incubated with a substochiometric amount of recombinant LKB1 in the presence of [γ-^{32}P]ATP. Proteins were separated by SDS–PAGE and subjected to autoradiography. ^{32}P was incorporated into the α1 and β1 subunits (β1A) and also into another hyperphosphorylated β1 species of slower electrophoretic mobility (β1B). (B) Autoradiographic fractionation profiles of phosphopeptides from the three peptide mixtures after in-gel digestion and microfractionation onto PACs. (C) Densitometric analysis of individual radioactive spots identified 11 distinguishable ^{32}P peaks derived from AMPK–α1. Although only two major ^{32}P peaks were observed for the regular β1 digest (β1A), at least five additional peaks were detected for the hyperphosphorylated β1 species (β1B).

Table 1
Identified AMPK phosphorylation sites.

AMPK	Spot	Phosphorylation site
α1	G9	ND
	G21	N-terminal His tag[a]
	I2	Ser475
	J21	Ser(483,485)[b]
	J17	Ser485 and Ser483[c]
	J1	Thr377
	K2	Thr377
	K5	Thr377
	K10	Thr172
	K22	ND
	L20	Ser349
β1A	A6	Ser24
	E5	Ser108
β1B	G20	Ser24
	H8	ND
	J12	Thr80
	J6	Ser174 or Ser177[d]
	K14	Thr158
	K16	ND
	K21	Ser108

Note. ND, no phosphopeptide detected.
[a] Peptide containing the N-terminal hexahistidine tag, including linker.
[b] Peptide phosphorylated at both residues.
[c] Two individual peptide species phosphorylated at either residue.
[d] Exact site of phosphorylation could not be identified.

(Fig. 4, spots I2 and I3; see also Supplementary MS Data S2). In contrast, 359 fmol of an unknown phosphopeptide proved to be too little for identification under the applied conditions (Fig. 4, spot J17). Apart from the benefit of absolute quantification for process optimization, the autoradiograph also reveals the relative stoichiometries of phosphorylation at the various sites (Fig. 4). However, it should be noted that the recovery of individual phosphopeptides from tryptic digests could vary significantly between species. Thus, although every precaution has been taken to minimize sample loss, relative quantification data should be interpreted with care.

Inhomogeneous distribution of phosphopeptides within individual PAC spots

As described above, autoradiography of the PACs revealed topologically inhomogeneous blackening for some spots. Most frequently, we observed an increased concentration of radiolabeled phosphopeptides at the peripheral rim of the spots, resulting in a ring-shaped blackening of the X-ray film. Therefore, we hypothesized that the phosphopeptide ion abundance in MS measurements might be crucially dependent on the phosphopeptide distribution within a spot. When these spots were manually analyzed by MS^2, we generally noticed an increased signal intensity of the isolated phosphopeptide in the rim area compared with the central area (Fig. 5). However, the most abundant signal intensities did not always coincide with the spot areas that contained the highest concentration of radiolabeled phosphopeptides. Rather, the manner of crystallization appeared to be a more critical parameter because the most efficient ionization of phosphopeptides was observed by laser bombardment of the densest crystal matrix regions (Fig. 5). To date, if running in automated mode, the laser movement follows only a defined geometrical pattern. The bright (high-density) areas are not distinguishable from the dark (low-density) areas in the crystal matrix by any of the currently available MALDI instrument setups. Implementation of matrix crystallization assessment to optimize laser positioning seems technically feasible and would only require the control software to use visual information from the camera. Alternatively, especially for very low amounts of peptides or those that are poorly ionized, the laser should be manually pointed to dense matrix areas for optimal analysis.

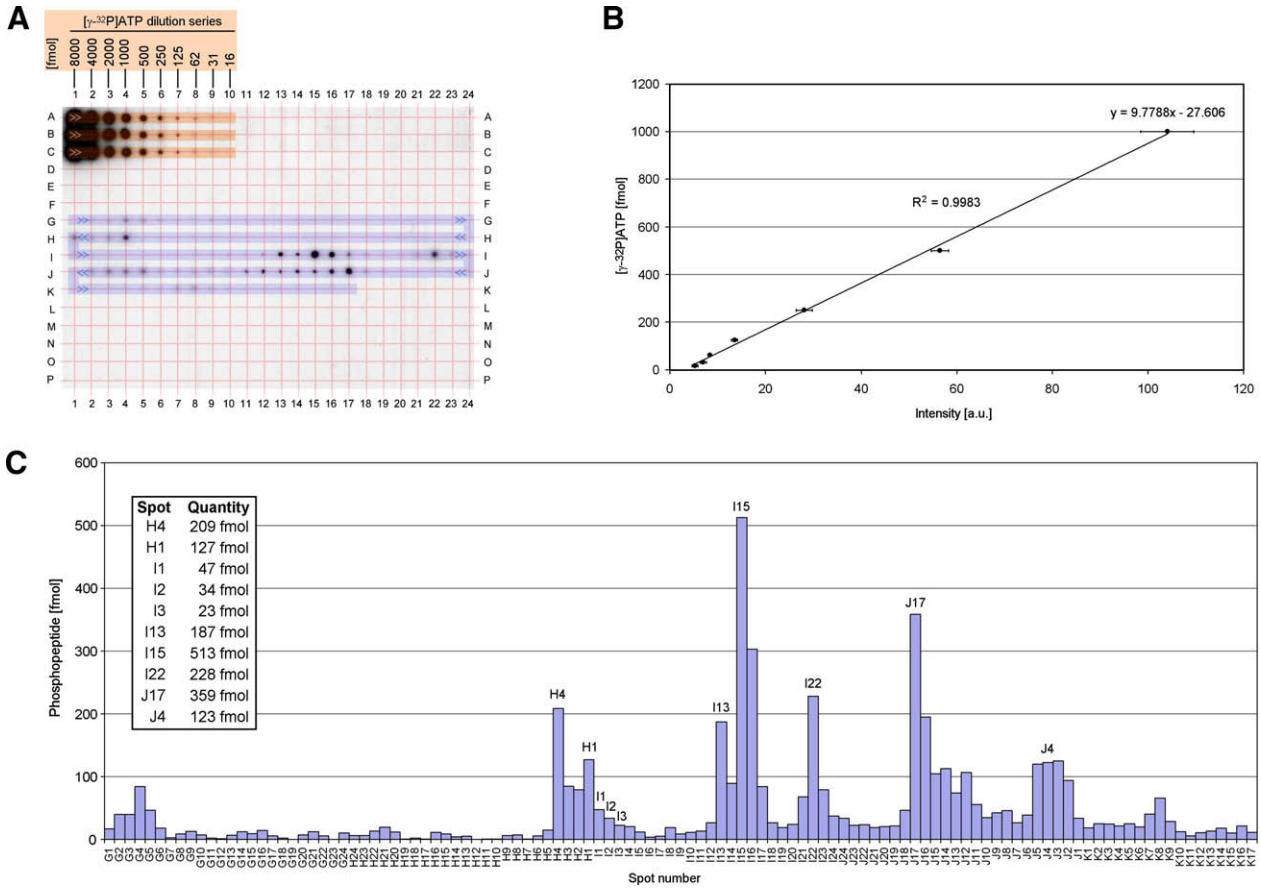

Fig. 4. Quantification of phosphopeptides derived from AMPK autophosphorylation of the α1 subunit. Following activation by LKB1, α1β1γ1–AMPK (2 μg, nontagged) was allowed to autophosphorylate in the presence of [γ-^{32}P]ATP. After tryptic in-gel digestion of the α1 subunit, half of the resulting peptides were fractionated by RPLC directly onto a PAC. (A) Autoradiograph of the PAC. The radiolabeled peptides were spotted from positions G1 to K17. In addition, a dilution series of the radioactive kinase buffer that was used in the phosphorylation assay was manually spotted in triplicate (A1–A10, B1–B10, and C1–C10). (B) Calibration curve for quantification of ^{32}P. Densitometric analysis of the dilution series revealed a nearly linear relationship between spot intensity and the amount of ^{32}P, with a coefficient of determination (R^2) of 0.9983. Error bars denote the standard deviations of each data point. a.u., arbitrary units. (C) Quantification of the phosphopeptides at the different PAC positions. By using the function of the regression line from (B), the absolute phosphopeptide amounts were back-calculated from the various spot intensities. The inset lists all spots and the corresponding quantities of the different phosphopeptides that, with the exception of spot J17, were successfully isolated for fragmentation in MS^2 mode. The relevant mass spectra are provided in Supplementary MS Data S2 (see supplementary material). Note that the elution profile differs slightly from the one in Fig. 3 because a nontagged α1 isoform of AMPK was used and a steeper acetonitrile gradient was applied in this experiment (see Materials and methods).

Conclusions

Here we have presented a workflow allowing tracking and quantification of phosphopeptides prior to analysis by MALDI MS. Despite considerable progress in the development of methods for phosphorylation site mapping, no single technique invariably allows complete isolation of all phosphopeptides in a complex sample. A recent study compared three common phosphopeptide isolation methods and showed that each of the techniques enriched a different set of phosphopeptides [31]. Moreover, even different instrumental setups can critically influence the identification of phosphorylation sites because some peptides are ionized more efficiently by either ESI or MALDI [32,33]. Hence, depending on the available equipment, practical know-how, and project-specific goals, the researcher must choose the most appropriate method(s). The focus of our analyses is on purified proteins; therefore, complexity of the sample is by definition low. On the other hand, a fully comprehensive dataset is most desirable because we want to avoid overlooking any phosphorylation sites of biological importance. Although nonradioactive MS-based methods have been continuously developed during recent years, it is noteworthy that the use of ^{32}P labeling in combination with MS remained constant [34]. Indeed, also in our hands, the use of radioactive phosphate for analysis of phosphopeptides remains advantageous because it allows tracking and quantification of the labeled peptide during all subsequent steps prior to identification by MS. In contrast to nonradioactive methods that are often used in conjunction with affinity-based approaches involving IMAC or titanium dioxide resins, the ^{32}P label clearly indicates the presence of phosphopeptides in a particular fraction even when these are not amenable to detection by MS. The visualization of phosphorylated peptides enables the researcher to focus any efforts to enhance phosphopeptide ionization and identification on selected spots only, thereby avoiding the waste of time on analysis of fractions containing no phosphorylated peptides. Furthermore, the use of radiolabels for incorporation into proteins during in vitro incubations also enables distinguishing between newly introduced and preexisting protein modifications resulting from in vivo targeting of the protein, which is complicating analysis and is common to proteins purified from eukaryotic sources.

Many laboratories prefer nonradioactive analytical methods due to safety issues and local policies and because the logistics of ^{32}P use vary by institution. The activity of the [γ-^{32}P]ATP stock solution is typically in the lower MBq range (i.e., above the exemption limit [LE] for licensing) and must be stored in a type C laboratory. When performing radioactive in vitro kinase assays, however,

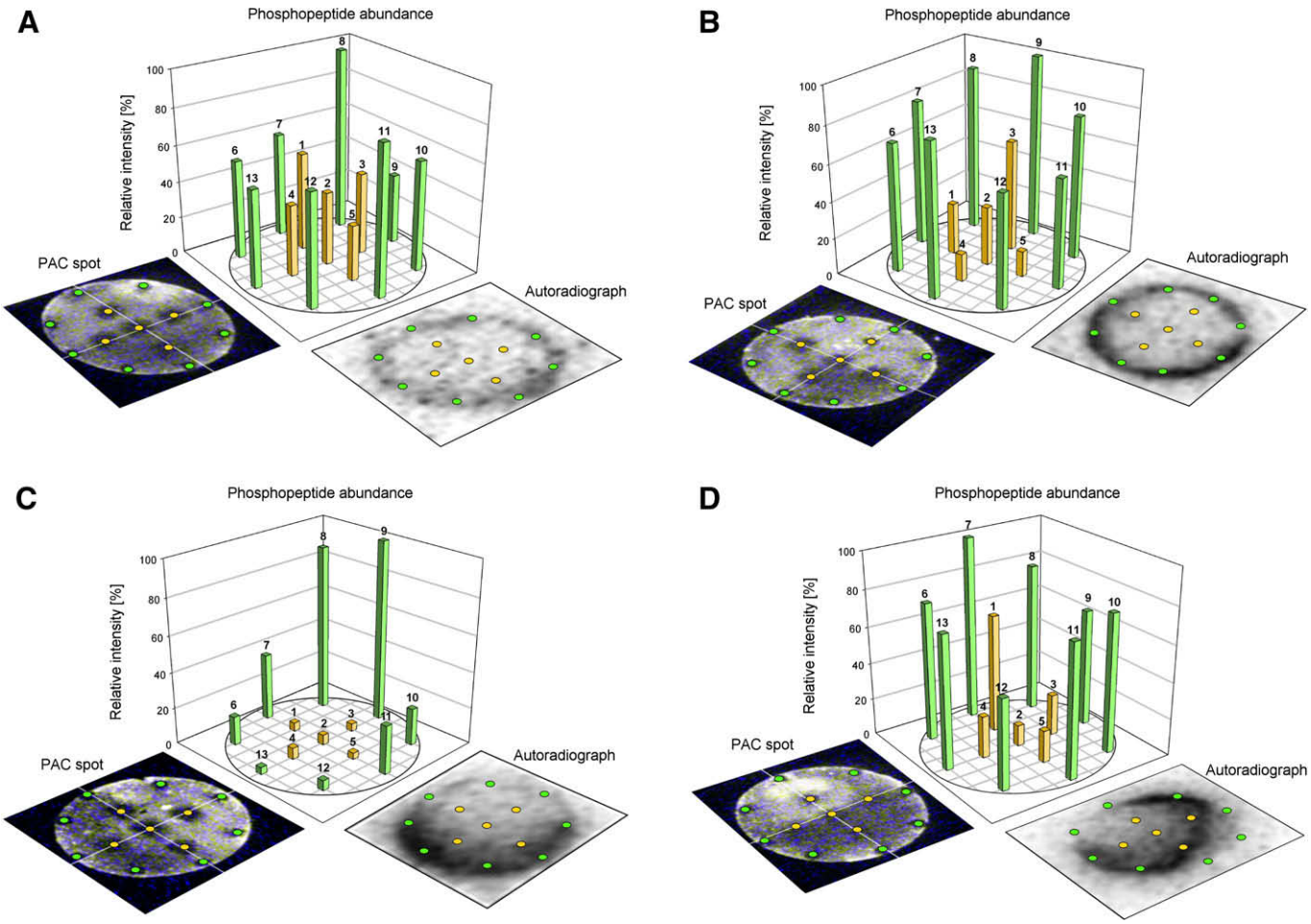

Fig. 5. Matrix crystallization is the major factor affecting phosphopeptide abundance in MS measurements. (A–D) Four spots of the PAC used for determination of AMPK–α1 phosphorylation sites (see Fig. 3) were analyzed in more detail in MS^2 mode. Importantly, all four spots were hitherto not subject to any MS measurements. However, they were located next to major phosphopeptide-containing spots that were previously analyzed by MS. (A) Spot I3, *m/z* 897.7. (B) Spot J15, *m/z* 963.3. (C) Spot K9, *m/z* 1845.6. (D) Spot K11, *m/z* 1845.6. The laser was locked into five inner positions (1–5, yellow) and eight outer positions (6–13, green) per spot. The laser power was kept constant for all measurements, and a total of 400 shots were accumulated per position. Bars represent the signal intensities of the isolated phosphopeptides that were recorded in the various positions within the individual spots. To provide an aid to orientation, these positions are marked with yellow and green circles in the autoradiograph and the charge-coupled device (CCD) image of each spot before and after laser bombardment, respectively. It is important to note that the black areas around the colored circles in the CCD image derived from the punctual laser bombardment of the crystal matrix. Irrespective of the actual phosphopeptide concentration, as indicated by the autoradiograph, more phosphopeptide was generally detected in the rim area of the spots compared with the central area. Moreover, the most abundant signal intensities were recorded in positions that displayed a crystal matrix of high density, that is, bright regions in the CCD image. Examples include position 8 in (A), position 9 in (B), position 9 in (C), and position 7 in (D). (For interpretation of the references to color in this figure legend, the reader is referred to the Web version of this article.)

the final working activity of ^{32}P is usually below the LE. Thus, apart from the storage of [γ-^{32}P]ATP, the presented workflow does not implicate particular infrastructural requirements. The in situ detection of phosphopeptides on the PAC relies on noncritical amounts of radioactivity even if one considers the ionizing MALDI conditions. Indeed, the typical activities, between 1 and 20 Bq per target plate, are approximately 1 million times below the annual limit of intake (14.8–33.3 MBq ^{32}P) as recommended by the U.S. Nuclear Regulatory Commission [35]. Consequently, we were unable to detect significant amounts of radioactivity when cleaning the MALDI source after regular use (MS and MS^2 measurements of ∼100 radioactive spots/month).

The combination of LC–MALDI MS^2 with autoradiographic imaging of the target plate allowed for identification of 10 distinct AMPK autophosphorylation sites. For only 1 of these sites the exact position of the phosphate remains undetermined. A similar analysis of AMPK phosphorylation sites using ^{32}P labeling, off-line RPLC, and nano-ESI MS^2 was reported previously and revealed just 3 autophosphorylation sites [18]. Although the latter study also fractionated tryptic, ^{32}P-labeled peptides derived from AMPK after in-gel digestion, the peptides eluted from the RP column were first collected in microfuge tubes, screened by liquid scintillation counting, and concentrated before MS analysis. Most likely, these manual processing steps entailed a considerable adsorptive sample loss, thereby preventing a substantial set of phosphopeptides from detection and identification. For the determination of phosphorylation sites by MALDI MS^2, the presented method offers attractive features, thereby enhancing existing techniques. As a result of the direct fractionation of phosphopeptides onto MALDI target plates and their detection by autoradiography in situ, sample loss due to repeated adsorption onto plastic surfaces is largely omitted. In terms of sensitivity, the in situ detection of phosphorylated peptides is superior to the popular liquid scintillation counting, thereby requiring minimal quantities of radioactivity and increasing operational safety.

Acknowledgments

We thank Ruedi Aebersold and Peter Hunziker for helpful discussions. This work was funded by the Swiss National Science

Foundation (3100A0-114137); ETH graduate student grants for R.D.T., R.F.T., and R.S.; and the FP-6 EU Framework Program (project LSHM-CT-2004-005272 EXGENESIS).

Appendix A. Supplementary data

Supplementary data associated with this article can be found, in the online version, at doi:10.1016/j.ab.2009.04.015.

References

[1] J.D. Graves, E.G. Krebs, Protein phosphorylation and signal transduction, Pharmacol. Ther. 82 (1999) 111–121.
[2] T. Hunter, Signaling—2000 and beyond, Cell 100 (2000) 113–127.
[3] T. Pawson, J.D. Scott, Protein phosphorylation in signaling—50 years and counting, Trends Biochem. Sci. 30 (2005) 286–290.
[4] M.J. Hubbard, P. Cohen, On target with a new mechanism for the regulation of protein phosphorylation, Trends Biochem. Sci. 18 (1993) 172–177.
[5] S. Zolnierowicz, M. Bollen, Protein phosphorylation and protein phosphatases, EMBO J. 19 (2000) 483–488.
[6] J.P. Blaydes, B. Vojtesek, G.B. Bloomberg, T.R. Hupp, The development and use of phospho-specific antibodies to study protein phosphorylation, Methods Mol. Biol. 99 (2000) 177–189.
[7] J.W. Mandell, Phosphorylation state-specific antibodies: applications in investigative and diagnostic pathology, Am. J. Pathol. 163 (2003) 1687–1698.
[8] J. Reinders, A. Sickmann, State-of-the-art in phosphoproteomics, Proteomics 5 (2005) 4052–4061.
[9] M. Mann, S.E. Ong, M. Gronborg, H. Steen, O.N. Jensen, A. Pandey, Analysis of protein phosphorylation using mass spectrometry: deciphering the phosphoproteome, Trends Biotechnol. 20 (2002) 261–268.
[10] G.L. Corthals, R. Aebersold, D.R. Goodlett, Identification of phosphorylation sites using microimmobilized metal affinity chromatography, Methods Enzymol. 405 (2005) 66–81.
[11] S.B. Ficarro, M.L. McCleland, P.T. Stukenberg, D.J. Burke, M.M. Ross, J. Shabanowitz, D.F. Hunt, F.M. White, Phosphoproteome analysis by mass spectrometry and its application to *Saccharomyces cerevisiae*, Nat. Biotechnol. 20 (2002) 301–305.
[12] C.E. Haydon, P.A. Eyers, L.D. Aveline-Wolf, K.A. Resing, J.L. Maller, N.G. Ahn, Identification of novel phosphorylation sites on *Xenopus laevis* Aurora A and analysis of phosphopeptide enrichment by immobilized metal-affinity chromatography, Mol. Cell. Proteomics 2 (2003) 1055–1067.
[13] W.J. Henzel, J.T. Stults, Matrix-assisted laser desorption/ionization time-of-flight mass analysis of peptides, Curr. Protoc. Protein Sci. (2001) unit 16.2.
[14] K.D. Speicher, O. Kolbas, S. Harper, D.W. Speicher, Systematic analysis of peptide recoveries from in-gel digestions for protein identifications in proteome studies, J. Biomol. Tech. 11 (2000) 74–86.
[15] I.I. Stewart, T. Thomson, D. Figeys, ^{18}O labeling: a tool for proteomics, Rapid Commun. Mass Spectrom. 15 (2001) 2456–2465.
[16] D. Neumann, A. Woods, D. Carling, T. Wallimann, U. Schlattner, Mammalian AMP-activated protein kinase: functional, heterotrimeric complexes by co-expression of subunits in *Escherichia coli*, Protein Expr. Purif. 30 (2003) 230–237.
[17] M. Suter, U. Riek, R. Tuerk, U. Schlattner, T. Wallimann, D. Neumann, Dissecting the role of 5′-AMP for allosteric stimulation, activation, and deactivation of AMP-activated protein kinase, J. Biol. Chem. 281 (2006) 32207–32216.
[18] A. Woods, D. Vertommen, D. Neumann, R. Turk, J. Bayliss, U. Schlattner, T. Wallimann, D. Carling, M.H. Rider, Identification of phosphorylation sites in AMP-activated protein kinase (AMPK) for upstream AMPK kinases and study of their roles by site-directed mutagenesis, J. Biol. Chem. 278 (2003) 28434–28442.
[19] S.C. Stein, A. Woods, N.A. Jones, M.D. Davison, D. Carling, The regulation of AMP-activated protein kinase by phosphorylation, Biochem. J. 345 (2000) 437–443.
[20] D. Neumann, M. Suter, R. Tuerk, U. Riek, T. Wallimann, Co-expression of LKB1, MO25α, and STRADα in bacteria yield the functional and active heterotrimeric complex, Mol. Biotechnol. 36 (2007) 220–231.
[21] S. Benvenuti, R. Cramer, C.C. Quinn, J. Bruce, M. Zvelebil, S. Corless, J. Bond, A. Yang, S. Hockfield, A.L. Burlingame, M.D. Waterfield, P.S. Jat, Differential proteome analysis of replicative senescence in rat embryo fibroblasts, Mol. Cell. Proteomics 1 (2002) 280–292.
[22] D. Suckau, A. Resemann, M. Schuerenberg, P. Hufnagel, J. Franzen, A. Holle, A novel MALDI LIFT–TOF/TOF mass spectrometer for proteomics, Anal. Bioanal. Chem. 376 (2003) 952–965.
[23] R.S. Annan, S.A. Carr, Phosphopeptide analysis by matrix-assisted laser desorption time-of-flight mass spectrometry, Anal. Chem. 68 (1996) 3413–3421.
[24] D.G. Hardie, AMP-activated protein kinase as a drug target, Annu. Rev. Pharmacol. Toxicol. 47 (2007) 185–210.
[25] D.G. Hardie, AMP-activated/SNF1 protein kinases: conserved guardians of cellular energy, Nat. Rev. Mol. Cell Biol. 8 (2007) 774–785.
[26] S.M. Warden, C. Richardson, J. O'Donnell Jr., D. Stapleton, B.E. Kemp, L.A. Witters, Post-translational modifications of the β-1 subunit of AMP-activated protein kinase affect enzyme activity and cellular localization, Biochem. J. 354 (2001) 275–283.
[27] S. Horman, D. Vertommen, R. Heath, D. Neumann, V. Mouton, A. Woods, U. Schlattner, T. Wallimann, D. Carling, L. Hue, M.H. Rider, Insulin antagonizes ischemia-induced Thr172 phosphorylation of AMP-activated protein kinase α-subunits in heart via hierarchical phosphorylation of Ser485/491, J. Biol. Chem. 281 (2006) 5335–5340.
[28] S. Kjellstrom, O.N. Jensen, Phosphoric acid as a matrix additive for MALDI MS analysis of phosphopeptides and phosphoproteins, Anal. Chem. 76 (2004) 5109–5117.
[29] H. Kuyama, K. Sonomura, O. Nishimura, Sensitive detection of phosphopeptides by matrix-assisted laser desorption/ionization mass spectrometry: use of alkylphosphonic acids as matrix additives, Rapid Commun. Mass Spectrom. 22 (2008) 1109–1116.
[30] C. Pan, S. Xu, H. Zhou, Y. Fu, M. Ye, H. Zou, Recent developments in methods and technology for analysis of biological samples by MALDI–TOF–MS, Anal. Bioanal. Chem. 387 (2007) 193–204.
[31] B. Bodenmiller, L.N. Mueller, M. Mueller, B. Domon, R. Aebersold, Reproducible isolation of distinct, overlapping segments of the phosphoproteome, Nat. Methods 4 (2007) 231–237.
[32] W.M. Bodnar, R.K. Blackburn, J.M. Krise, M.A. Moseley, Exploiting the complementary nature of LC/MALDI/MS/MS and LC/ESI/MS/MS for increased proteome coverage, J. Am. Soc. Mass Spectrom. 14 (2003) 971–979.
[33] N. Li, N. Wang, J. Zheng, X.M. Liu, O.W. Lever, P.M. Erickson, L. Li, Characterization of human tear proteome using multiple proteomic analysis techniques, J. Proteome Res. 4 (2005) 2052–2061.
[34] K.M. Loyet, J.T. Stults, D. Arnott, Mass spectrometric contributions to the practice of phosphorylation site mapping through 2003: a literature review, Mol. Cell. Proteomics 4 (2005) (2003) 235–245.
[35] US Nuclear Regulatory Commission, Standards for protection against radiation, NRC Regulations Title 10, Code of Federal Regulations (10 CFR), part 20, 2008.